AGU100 ADVANCING EARTH AND SPACE SCIENCE

JGR

Journal of Geophysical Research: Oceans

RESEARCH ARTICLE

10.1029/2017JC013638

Key Points:

- Sediment-acoustic relationships were modeled from multibeam backscatter and sediment data in four different areas on the Australian margin
- Sediment mud content and mean grain size have significant negative and positive relationships with acoustic backscatter intensity, respectively
- The strongest backscatter return occurs with medium sediment mud content and large mean grain sizes

Supporting Information:

- Supporting Information S1
- Data Set S1

Correspondence to:
Z. Huang,
zhi.huang@ga.gov.au

Citation:
Huang, Z., Siwabessy, J., Cheng, H., & Nichol, S. (2018). Using multibeam backscatter data to investigate sediment-acoustic relationships. *Journal of Geophysical Research: Oceans*, *123*, 4649–4665. https://doi.org/10.1029/2017JC013638

Received 19 NOV 2017
Accepted 31 MAY 2018
Accepted article online 20 JUN 2018
Published online 5 JUL 2018

Using Multibeam Backscatter Data to Investigate Sediment-Acoustic Relationships

Zhi Huang[1,2], Justy Siwabessy[2], Heqin Cheng[1], and Scott Nichol[2]

[1]State Key Laboratory of Estuarine and Coastal Research, East China Normal University, Shanghai, China, [2]National Earth and Marine Observations Branch, Geoscience Australia, Canberra, ACT, Australia

Abstract Sediment properties are known to influence acoustic backscatter intensity. This sediment-acoustic relationship has been investigated previously through using physical geoacoustic models and empirical methods and found to be complex and nonlinear. Here we employ a robust machine-learning statistical model (random forest decision tree) to investigate the most likely nonlinear sediment-backscatter relationships. The analysis uses colocated sediment and acoustic backscatter data (collected from a 300-kHz multibeam sonar system) for 564 locations in four different areas on the Australian margin. Seven sediment grain size properties (%gravel, %sand, %mud, mean grain size, sorting, skewness, and kurtosis) were used to predict the acoustic backscatter responses at individual incidence angles. The modeling results demonstrate the effectiveness of this multivariate predictive approach for the investigation of sediment-acoustic relationship. Thus, we find that for incidence angles between 1° and 41°, the sediment variables explain around 70% of variance in the backscatter intensity. Sediment mud content was found to be the most important sediment variable in the model and has a significant negative relationship with backscatter intensity. Mean grain size was the second ranked sediment variable and found to have a positive relationship with backscatter intensity. The results also show that sediment mud content plays a key role in sorting-backscatter and sand-backscatter relationships. Using only two sediment properties, mud content and mean grain size, together it was possible to largely explain the sediment-acoustic relationship. The strongest backscatter return occurred with medium sediment mud content and large mean grain sizes (or muddy coarse sand).

1. Introduction

Traditionally, seabed sediment information was only available from a limited number of samples collected during marine surveys. With the rapid development of acoustic remote sensing technologies in side scan sonar and multibeam echo sounder, seabed sediment characteristics and substrate types can now be effectively mapped by proxy across large areas (Anderson et al., 2008; Pratson & Edwards, 1996). This technological advance chiefly relies on the ability of acoustic backscatter data to broadly differentiate sediment types, principally mud, sand, and gravel (e.g., Huang et al., 2013; Lucieer, 2008).

Physically based geoacoustic models, such as the composite roughness model, have been developed to investigate the sediment-acoustic relationship (APL-UW, 1994; Fonseca et al., 2002; Hamilton, 1980; Jackson et al., 1986; Jackson & Briggs, 1992). Previous studies using these physical models demonstrated that sediment grain size properties and various substrate types can be distinguished based on their backscatter angular response curves (APL-UW, 1994; Chakraborty et al., 2000; De & Chakraborty, 2011; Fonseca et al., 2002; Fonseca & Mayer, 2007; Haris et al., 2011). However, due to the large variability of seabed properties across the global oceans, one single geoacoustic model is not likely applicable to all cases (Hamilton, 1980; Hughes Clarke, 1994). The sediment-acoustic relationship is thus often investigated through empirical and statistical approaches. Numerous studies have indicated that acoustic backscatter strength correlates with sediment grain size properties (Collier & Brown, 2005; Davis et al., 1996; De Falco et al., 2010; Ferrini & Flood, 2006; Goff et al., 2000, 2004; Haris et al., 2012; Huang et al., 2012; Huang, Siwabessy, et al., 2014; Kloser et al., 2001; Ryan & Flood, 1996; Sutherland et al., 2007), and backscatter data can be used to classify substrate types (Hamilton & Parnum, 2011; Huang et al., 2013; Lucieer, 2008; Lucieer & Lamarche, 2011; McGonigle et al., 2009; Preston, 2009; Rzhanov et al., 2012). For example, studies showed that backscatter intensity has a moderate and positive correlation with sediment mean grain size (MGS; Collier & Brown, 2005; Davis et al., 1996; Ferrini & Flood, 2006; Goff et al., 2000; Huang, Siwabessy, et al., 2014; Ryan & Flood, 1996). Also, backscatter intensity was found to be positively correlated with coarse fractions and inversely correlated with finer fractions of the sediment composition (De Falco et al., 2010; Goff et al., 2004; Haris et al., 2012; Huang, Siwabessy, et al., 2014; Sutherland et al., 2007). Other sediment grain size properties, especially sorting may also play important roles in the backscatter-sediment relationship (Ferrini & Flood, 2006; Goff et al., 2004; Goff et al., 2000; Huang et al., 2012; Huang, Siwabessy, et al., 2014).

In most of the above-mentioned studies, acoustic backscatter response was simply correlated with one particular sediment grain size property, such as MGS. Although this univariate analysis is useful for the understanding of the sediment-acoustic relationship, it is not sufficient for the in-depth understanding of the mechanisms behind the complex sediment-acoustic relationship briefly described in the next section. Huang et al. (2012) and Huang, Siwabessy, et al. (2014) have used acoustic backscatter data (as the explanatory variables) to model multiple sediment grain size properties (as the response variables). This approach is useful for seabed mapping but not so for the understanding of sediment-acoustic relationships. To our knowledge, only one study applied a multivariate linear regression method to investigate the acoustic backscatter response (e.g., as the response variable) due to the interaction of several sediment properties (e.g., as the explanatory variables; Ferrini & Flood, 2006). Note that this statistical approach is the reverse of that of Huang et al. (2012) and Huang, Siwabessy, et al. (2014).

This study aims to employ a similar multivariate approach for the investigation of sediment-acoustic relationships. Seven sediment grain size properties, %gravel, %sand, %mud, MGS, sorting, skewness, and kurtosis, are used as explanatory variables (or predictors) to predict the acoustic backscatter responses at individual incidence angles (the response variables). We employ a robust machine-learning statistical model to investigate the most likely nonlinear sediment-backscatter relationships, based on colocated sediment and acoustic backscatter data, which was collected using a 300-kHz multibeam sonar system, from four areas on the Australian margin. These areas represent different sedimentary environments, ranging from sand-dominated nearshore to mixed mud, sand and gravel shelf deposits.

2. Sediment-Acoustic Relationship

The backscatter intensity received by an acoustic device (or a transducer) is a function of the signal absorption and scattering properties of water, the interaction with the water-seabed interface, the angle of incidence, and seabed topography (de Moustier & Matsumoto, 1993). After radiometric and geometric corrections, the calibrated backscatter data reflect the acoustic properties of water-seabed interface such as interface roughness parameters, water and sediment densities, sediment porosity, water and sediment sound velocities, and the sound attenuation coefficient in sediment (Hamilton, 1980; Jackson et al., 1986; Jackson & Briggs, 1992). In general, these acoustic properties vary with the seabed substrate types (Hamilton, 1980). More specifically, after calibration, the backscatter intensity is largely a function of incidence angle and three seabed physical properties: the acoustic impedance contrast (often called *hardness*), apparent interface roughness (relative to acoustic frequency), and sediment heterogeneity (Ferrini & Flood, 2006; Fonseca & Mayer, 2007; Jackson & Briggs, 1992; Jackson et al., 1986; Kloser et al., 2001; Lurton & Lamarche, 2015).

When encountering the water-seabed interface, a portion of the incidence acoustic energy reflects and scatters from the seabed, the remaining portion penetrates into the seabed. The acoustic impedance is defined by the product of density and sound velocity. Harder seabed interfaces (e.g., hard substrate and coarse sediment), which have a higher impedance contrast to water, return higher acoustic energy to the transducer. Interface roughness is caused by small-scale bathymetric relief. Smooth seabeds generate specular reflection in directions away from the transducer at oblique incidence angles. As a result, the transducer receives little returned acoustic energy at this angle range; but at near-nadir incidence angles, the returned acoustic energy is the strongest. In contrast, rougher seabed scatters the incidence energy at all directions, which effectively returns more energy back to the transducer. It should be noted that the effect of seabed (interface) roughness is often acoustic frequency dependent; for the frequency range used by modern multibeam echo sounders (tens to hundreds of kilohertz), the same seabed appears rougher to higher acoustic frequency. Volume scattering occurs when acoustic energy penetrates into the seabed. The amount of penetration is dependent on the acoustic frequency and interface hardness. Hard substrates (e.g., rocks) result in little penetration. For sediment, with decreasing hardness, a higher portion of the incidence energy is transmitted into the sediment. Meanwhile, higher frequency results in less penetration depth. The transmitted acoustic energy into the sediment is scattered by the heterogeneity of the sediment; a portion of this volume scattering eventually returns to the transducer. Generally, the contribution from volume scattering to backscatter intensity is higher for more heterogeneous sediment.

Importantly, seabed backscatter strength is also angle dependent (de Moustier & Alexandrou, 1991; Jackson et al., 1986; Lurton & Lamarche, 2015). At near-nadir incidence angles, the contribution from vertically specular reflection dominates the backscatter return, which usually results in the highest intensity, although this decreases very quickly with soft sediment (Ferrini & Flood, 2006; Jackson et al., 1986). However, at oblique incidence angles, contributions from interface roughness and volume scattering dominate (Ferrini & Flood, 2006; Jackson et al., 1986). At higher incidence angles (e.g., greater than the critical angle), little acoustic energy is transmitted into sediment, and the contribution from interface roughness also decreases quickly (Jackson et al., 1986; Jackson & Briggs, 1992).

3. Study Areas

Four study areas are used to provide a range of seabed sediment types (Figure 1):

1. Jervis Bay, situated on the south coast of New South Wales, is a semienclosed coastal embayment. The bay is exposed to highly variable offshore seas and swell from the southeast that is attenuated through the entrance and across subtidal reefs and shoals. Tidal range is microtidal (mean range ~1.6 m) with tidal currents weak, apart from at the entrance (Holloway et al., 1992). Seabed samples used for this study were collected from the southeastern part of Jervis Bay where the sediment comprises fine-medium quartz sand with minor carbonate content (Anderson et al., 2009; Taylor, 1972). Water depths in the survey area range from <5 to 40 m.
2. Joseph Bonaparte Gulf, on the northern Australian margin, is an extensive, shallow carbonate-dominated shelf characterized by carbonate banks and terraces (Heap et al., 2010; Przeslawski et al., 2011). The gulf receives significant loads of fine-grained sediment from the numerous rivers in this tropical part of Australia that are mixed with locally produced carbonate sediments (Lees, 1992). Tidal range is upper-meso (~2–5 m) with strong tidal currents acting to transport suspended sediments across the shelf. The region is also influenced by cyclones that generate waves that may initiate sediment transport across the shallower banks and terraces (i.e., <20 m). Mapping and sampling were undertaken across four survey areas in the outer Gulf in water depths of 20 to 200 m. The sampled sediment is overwhelmingly composed of carbonate grains, with textures ranging from well-sorted coarse-to-medium sand to very poorly sorted sandy mud.
3. Oceanic Shoals, located to the northwest of Joseph Bonaparte Gulf, is characterized by isolated carbonate banks and terraces, separated by submarine plains and channels (Nichol et al., 2013). The area also receives sediment discharged from coastal river systems. Strong tidal flows, locally generated wind driven waves, and seasonal cyclones all have influence on sediment transport. Four areas were surveyed within this study site in water depths of 30 to 180 m. Seabed sediment samples comprise well-sorted silt to sandy silt on plains to poorly sorted coarse muddy sand, sometimes with gravel inclusions on banks and terraces (Nichol et al., 2013).
4. Carnarvon shelf, located along the central coast of Western Australia, is characterized by a mix of sandy seabed with mobile bedforms and hard-ground areas comprising shore-parallel ridges, mounds, and irregular rocky outcrops (Brooke et al., 2009; Nichol & Brooke, 2011). The shelf experiences a strongly seasonal wave climate, ranging from low-energy (calm) summer conditions to high-energy storms in winter (wave height 3–4 m), with summer cyclones approximately every 2 years. Tidal range is microtidal (~0.6–1.8 m) and tidal currents weak, but regional oceanographic currents (Leeuwin Current and Ningaloo Current) are strong enough to initiate sand transport. Seabed sediments were sampled across three survey areas in water depths of 30 to 250 m (Huang, McArthur, et al., 2014). In the northern survey area, the sediment ranges from gravelly sand on the inner shelf to sand and muddy sand on the middle and outer shelf. In the central survey area, the sediment comprises varying mixtures of mud, sand, and gravel but within an overall trend of increased mud content toward the outer shelf. Sediment in the southern survey area is dominated by sand, with a small proportion of gravel on the middle and outer shelf.

10.1029/2017JC013638

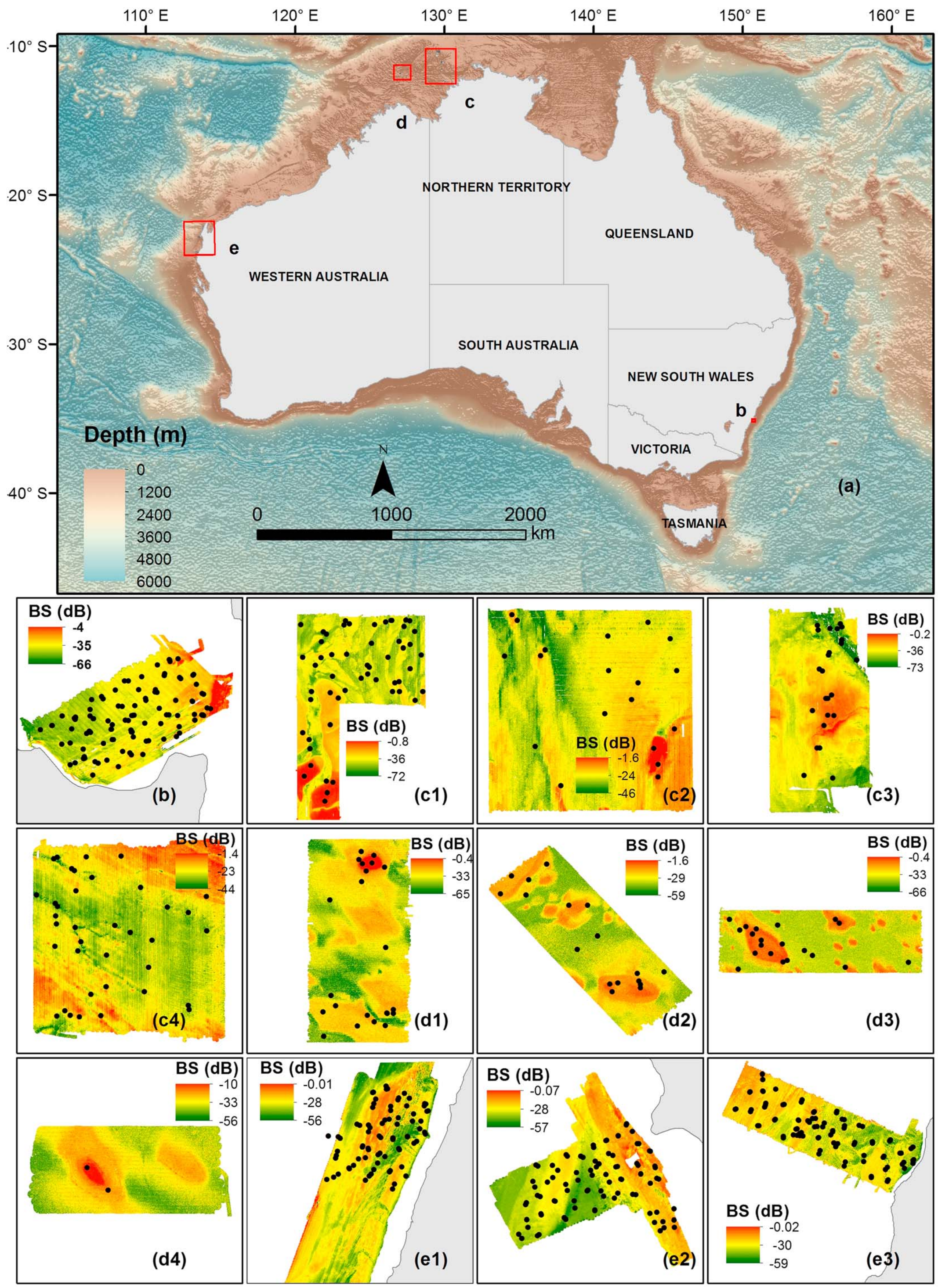

Figure 1. The study areas and the sample locations overlaid on the multibeam backscatter mosaics normalized at 25° incidence angle; (a) the locations of the study areas on the Australian margin; (b) the Jervis Bay survey area; (c1–c4) the four subareas within the Joseph Bonaparte Gulf survey area; (d1–d4) the four subareas within the Oceanic Shoals survey area; (e1–e3) the three subareas within the Carnarvon Shelf survey area.

4. Materials and Methods

4.1. Acoustic Backscatter Data

Acoustic backscatter data were collected as part of seabed mapping and sampling surveys in each of the four study areas, using a 300-kHz Kongsberg EM3002 multibeam sonar system. For each data set, raw backscatter data were calibrated and processed using CMST-GA MB Process v8.11.02.1 software, a multibeam backscatter processing toolbox codeveloped by Geoscience Australia and the Centre for Marine Science and Technology at Curtin University of Technology (Gavrilov, Duncan, et al., 2005; Gavrilov, Siwabessy, & Parnum, 2005; Parnum & Gavrilov, 2011a). For each survey the system was calibrated against a reference seabed to make sure the backscatter level consistent across surveys. The reference seabed for each survey was chosen at a uniform, sandy and flat location, consistent with the recommendation of Lamarche and Lurton (2017). Backscatter processing included correction for transmission loss and ensonification area, and removal of the system implemented model and the angular dependence (Siwabessy et al., 2017).

Essentially, the backscatter processing involves applying a generalized sonar equation to the calibration process (equation (1); the expanded equations can be found in ICES, 2007, and Parnum and Gavrilov, 2011a):

$$\overline{Ss(\theta i)} = EL(\theta i) - SL(\theta i) + 2TL(\theta i) - 10\log\overline{A(\theta i)} \quad (1)$$

where $\theta_{i;}$ is the incidence angle, $\overline{S_s(\theta_i)}$ is the averaged backscatter strength, *EL* (θ_i) is the echo level, *SL* (θ_i) is the source level including directivity, *TL* (θ_i) is the transmission loss in the water column, and $\overline{A(\theta_i)}$ is the ensonification area. In the raw data, the manufacturer implements a system model to produce an equalized backscatter mosaic by removing the angular dependence of the backscatter strength (Hammerstad, 2000). It is essential that this model be removed in order to revert back the true relationship between backscatter intensities and incidence angles. Therefore, beside the corrections defined by equation (1) (e.g., the transmission loss and ensonification area), the process within the toolbox also removes the system model and involves the calculation of the incidence angle and correction of the beam pattern.

After all corrections, 60 backscatter mosaics gridded from incidence angles of 1° to 60° were generated at an interval of 1°. Each individual backscatter mosaic contains angularly equalized backscatter strengths that were normalized to the backscatter strength at a particular incidence angle (Parnum & Gavrilov, 2011b). Effectively, we used an along-track sliding window of 100 pings to calculate the mean angular response within the window; this mean angular trend was then removed and the mean backscatter value within the window at one of the chosen incidence angles between 1° and 60° was added back to generate the normalized backscatter at the chosen incidence angle (Parnum & Gavrilov, 2011b). Using this empirical method (Parnum & Gavrilov, 2011b), we were able to generate backscatter mosaics at all incidence angles for all study areas. This would enable us to investigate whether the sediment-backscatter relationships are affected by acoustic incidence angle without explicitly using backscatter angular response curve (e.g., Huang et al., 2013; Huang, Siwabessy, et al., 2014; Lamarche et al., 2011). The spatial resolution of these backscatter mosaics are 2 m for Jervis Bay and Oceanic Shoals, 3 m for Carnarvon Shelf, and 10 m for Joseph Bonaparte Gulf.

It is important that we maintain backscatter level consistent across surveys (Lamarche & Lurton, 2017). For every survey in this study, the backscatter level was monitored using the build-in self-test procedure as part of mobilization and calibration procedure at the beginning of a survey. The backscatter data were collected over a known seabed type (e.g., sand). Measured backscatter data were compared to the APL-UW theoretical model of the seabed type (APL-UW, 1994). Any residuals between the measured backscatter data and the theoretical model were removed from the measured backscatter so that the calibrated backscatter data matches the theoretical model. This is part of the beam pattern correction mentioned earlier, similar to the calibration process implemented in Lamarche et al. (2011) to fit a modeled pattern on data recorded over homogenous seabed. Backscatters from any overlapping areas between surveys were also monitored. Lastly, we maintained the same settings (e.g., ping mode, pulse length, transmitter power, and receiver gain) for all our surveys in order to maintain backscatter level consistent across surveys, similar to the recommendation of constancy of acquisition settings by Lamarche and Lurton (2017). We applied minimum changes to the settings only when survey conditions demand.

This standard multibeam acquisition and instrument calibration procedure (Buchanan et al., 2013), together with the standard backscatter processing method, have ensured the consistency of the relative backscatter

Table 1
Summary Statistics for All Sediment Samples (n = 564) Used in This Analysis

Statistic	%Gravel	%Sand	%Mud	MGS (μM)	Sorting (μM)	Kurtosis	Skewness
Min	0.00	0.95	0.00	8.87	12.23	−0.44	−0.55
Max	96.18	100.00	99.05	1113.27	630.67	109.31	9.11
Mean	12.11	75.78	12.11	436.49	308.89	4.97	1.23
SD	17.55	23.51	18.44	213.69	128.64	6.69	0.88

Note. SD = standard deviation; MGS = mean grain size.

calibration (Lamarche & Lurton, 2017). As a result, the decibel values from all backscatter mosaic images across the four study areas are indeed comparable.

4.2. Sediment Samples

Sediment samples were collected from a range of water depths (5–200 m) using a Smith-McIntyre grab (10 L, 0.1-m^2 opening) from representative areas of seabed in each survey. Sample collection occurred at the same time as the multibeam surveys with sample location determined using the same DGPS system as the multibeam surveys. The grain size properties of these samples were analyzed in the laboratory to determine the following: %mud, %sand, and %gravel by wet sieve separation (Lewis & McConchie, 1994); MGS; sorting, standard deviation, SD; skewness and kurtosis on the sand and mud fractions by laser granulometry (using a Malvern Mastersizer 2000) with summary statistics calculated using GRADISTAT (Blott & Pye, 2001). In total, we used data from 564 sediment samples that collectively provide a broad textural range from mud to gravel (Table 1).

4.3. Statistical Modeling

For each sediment sample, the mean backscatter intensity values within a circular buffer of 30-m radius around the sample location were extracted from the backscatter mosaics. This buffer was to account for the positional uncertainty of the sediment samples. It is also reasonable to assume that the sediments within these small buffers are relatively homogenous because we only chose representative areas of seabed to sample. The sediment and acoustic backscatter data set of the 564 sediment samples used in this study is available in the supporting information (Data Set S1). Statistical modeling was then undertaken using the random forest decision tree (RFDT; Breiman, 2001) technique, implemented through DTREG software (http://www.dtreg.com), to investigate the sediment-acoustic relationship. The RFDT grows a number of independent (single) decision trees (e.g., the classification and regression tree, Breiman et al., 1984) in parallel. The predictions of these individual trees are combined through a bagging (Bootstrap Aggregating) process. The aggregation is done either by averaging (regression) or by majority voting (classification) to generate the final prediction. The bootstrap involves randomly selecting a proportion of samples with replacement from the entire sample set for each of the individual trees. In addition, the RFDT also chooses a random number of predictors (explanatory variables) from the entire predictor set for each of the individual trees. These two randomization processes encourage diversity (variation) among individual trees, which often improves prediction performance over that of a single decision tree.

The RFDT's robust modeling performance and ability to identify and rank explanatory variables (e.g., Francke et al., 2008; Huang et al., 2012; Huang, Siwabessy, et al., 2014) were the main reasons behind its selection as the statistical modeling technique of this study. In this study, we developed 60 RFDT models corresponding to 60 mosaics normalized to the backscatter intensity at 60 different incidence angles. The seven sediment grain size properties were the explanatory variables in all of the 60 models, while the response variables were the backscatter intensity values derived from the individual mosaics normalized to the backscatter intensity at 60 incidence angles. The statistical performance of the RFDT models was evaluated using the bagging process (Breiman, 2001). When constructing each tree in the forest, about two thirds of the randomly selected samples (in-bag samples) were used to build the tree; while the remaining one-third of samples (out-of-bag, or OOB samples) were reserved for error assessment. These OOB predictions were aggregated by averaging across all trees in the forest to give the overall prediction accuracy for the RFDT model.

To optimize the modeling performance, RFDT was used within a manual model selection process. After a process of trial-and-error, the following RDFT parameters were set:

- Number of trees in the forest: 1000
- Maximum tree levels: 10
- Minimum size node to split: 5
- Random predictor control: square root of total predictors

The manual feature selection process, which is an iterative process, searched for the best combination of explanatory variables that maximize the prediction accuracy. In the first iteration, only one (out of seven) explanatory variable was added to the RFDT model. This was repeated for all seven explanatory variables one by one. The explanatory variable for which we obtained the highest prediction accuracy (adjusted R^2) was retained in the RFDT model for the next iteration, and the accuracy value was recorded. Similarly, in the second iteration, we iteratively added one of the remaining six explanatory variables to the RFDT model and chose the one that achieved the highest prediction accuracy. Each of the following iterations selected a different explanatory variable from the remaining explanatory variables. The iteration process was stopped when there was either no further improvement in prediction accuracy or all explanatory variables had been added to the model, whichever happened first. For each response variable, the final RFDT model was the one using the best combination of explanatory variables.

4.4. Important Sediment Variables and Sediment-Backscatter Curves

RFDT has the ability to identify and rank the importance of the explanatory variables (e.g., the sediment grain size properties in this study). This is achieved by summing the improvement in accuracy gained by each split that used the explanatory variable. The importance score (IS) for the most important explanatory variable is assigned a value of 100. Other explanatory variables have lower scores, scaled accordingly (Sherrod, 2008). For the important explanatory variables, we can construct predicted relationship curves between them and the response variables (e.g., acoustic backscatter intensity at individual incidence angles). The purpose of these curves is to help the interpretation of modeled relationships in a quantitative way (Gogina et al., 2010; Huang et al., 2012; Huang, Siwabessy, et al., 2014). In this study, the relationship curves (e.g., sediment-backscatter curves) were predicted only for those sediment properties with ISs greater than 50.

For each of the seven sediment grain size properties, we constructed an artificial data set to predict the sediment-backscatter relationship curves. The artificial data set had 101 rows and 7 columns. Using the %gravel variable as an example, the column for the %gravel attribute has values ranging from its minimum (i.e., 0) to its maximum values (i.e., 100) with equal increments. The minimum and maximum values were obtained either from the sediment samples (e.g., for MGS, sorting, kurtosis, and skewness variables; Table 1) or from the theoretically lowest and highest bounds (e.g., for the %mud, %sand, and %gravel variables). The value of any of the remaining columns was kept constant as the mean value of the respective sediment grain size property. The artificial data set was then fed to the selected final RFDT model to predict the acoustic backscatter intensity as a function of %gravel.

5. Results

5.1. Univariate Analysis

The relationships between the seven sediment variables and the backscatter intensity from the mosaic normalized to the backscatter intensity at incidence angle of 25° are shown in Figure 2. These plots were fitted with one of three functions: linear, polynomial, or logarithmic (for least squares fits). Among these relationships, the strongest correlation occurs between %mud and the backscatter intensity (R^2 = 0.51), which indicates a clear negative relationship when fitted with a polynomial function, whereas the relationship between MGS and backscatter intensity is also strong but positive, with R^2 = 0.41. The skewness parameter and %sand also have notable correlations with the backscatter intensity, with negative and positive correlations, respectively. Kurtosis and sorting have relatively weak relationships with the backscatter intensity. In contrast, there is a very weak correlation between %gravel and the backscatter intensity (R^2 = 0.06; Figure 2a). Univariate analyses from other incidence angles indicate similar sediment-backscatter relationships and thus are not detailed here.

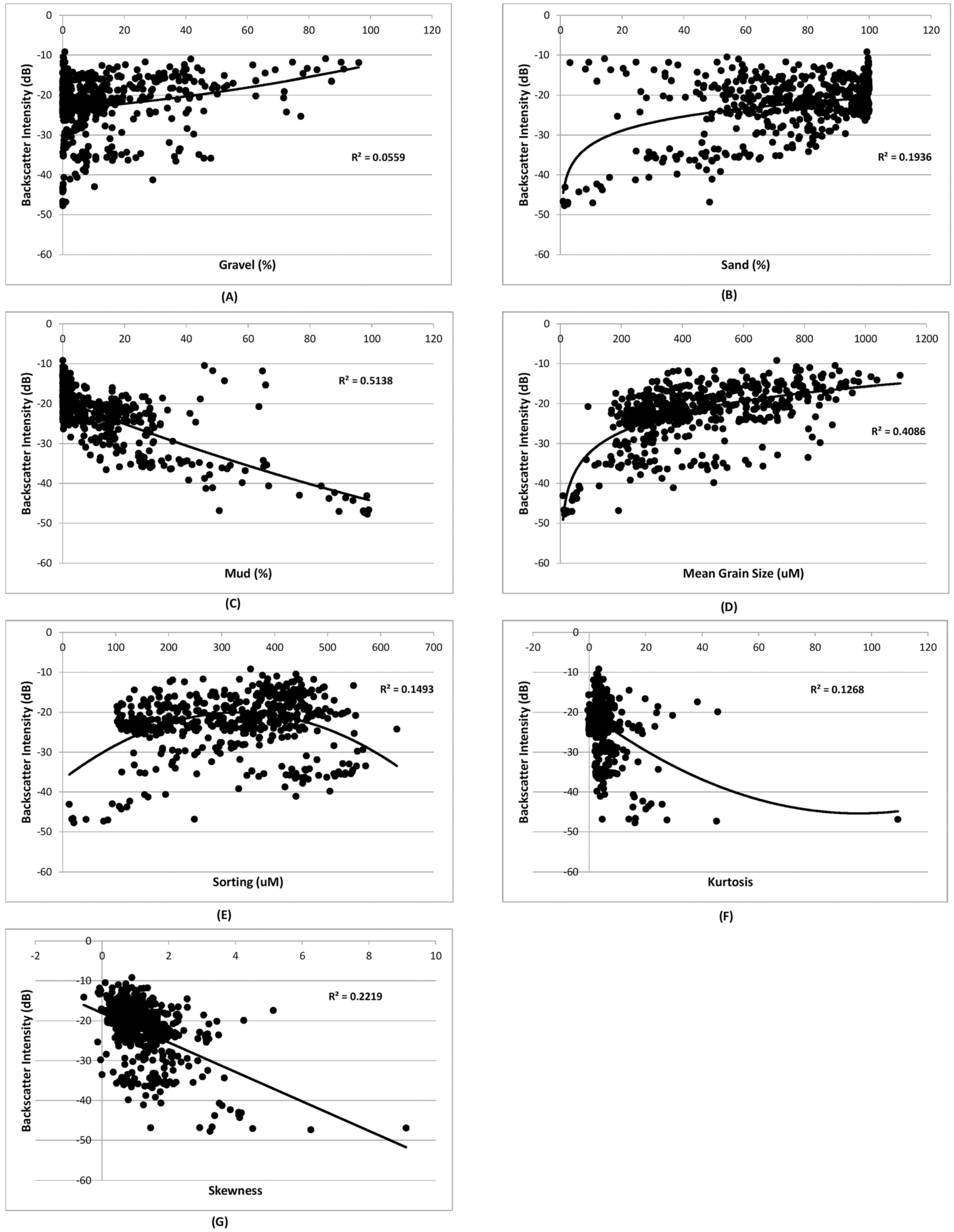

Figure 2. Univariate analysis; (a) gravel (polynomial fitting); (b) sand (logarithmic fitting); (c) mud (polynomial fitting); (d) mean grain size (logarithmic fitting); (e) sorting (polynomial fitting); (f) kurtosis (polynomial fitting); (g) skewness (linear fitting).

5.2. Modeling Results

For incidence angles between 1° and 41°, the RFDT models achieved fairly good performance based on the OOB assessment, with percentages of variance explained around 70% (Figure 3). The model's predictive performance gradually decreased for the outer beam range (incidence angle > 41°), until reaching the minimum of 48% variance explained at the incidence angle of 58°.

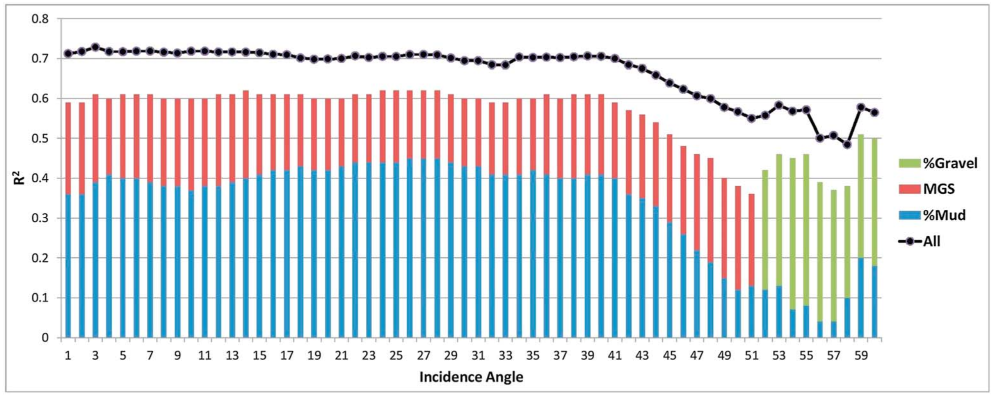

Figure 3. The percentages of variance explained (R^2s) based on the out-of-bag assessment of the 60 random forest decision tree models. The line indicates the R^2s of the final models. The bars indicate the R^2s from the models that used only first two sediment variables selected by the manual feature selection process. MGS = mean grain size.

The results of the manual feature selection process show that both %mud and sorting variables have been selected in all 60 RFDT models (Table 2). The sediment variables of %gravel, kurtosis, and MGS were also frequently included. The %sand variable was selected over 50% of the time, while the skewness variable was rarely used in the final models. The final RFDT models used between four and six (out of seven) sediment variables to achieve the highest predictive accuracy.

The %mud variable was consistently identified as the most important sediment variable controlling the backscatter response at all incidence angles (Table 2). Between incidence angles of 3° and 51°, the RFDT identified the MGS variable as second ranked, with a mean IS of 61.3. Outside this range of incidence angles, the sorting variable was more likely to be the second ranked parameter. Overall, the %mud variable was most important; the MGS variable was the second most important (*Mean IS* in Table 2). This was followed by the sorting variable, then the kurtosis, %gravel, and %sand variables. The skewness variable was not important at any incidence angle.

5.3. Predicted Sediment-Backscatter Curves

Here we present sediment-backscatter modeled curves for those variables ranked as important in the RFDT modeling process (i.e., IS $>$ 50). Thus, for the %mud-backscatter relationship we find the predicted curves from all 60 RFDT models show similar shapes within a standard deviation from the mean of ~4 dB (Figure 4a). This curve indicates a negative but nonlinear relationship, whereby with increasing mud content the backscatter intensity decreases. The total reduction is around 12 dB.

The MGS variable was identified by the RFDT models as an important sediment variable for backscatter response between incidence angles of 2° and 51°. Again, the predicted MGS-backscatter curves from these 50 models show similar shapes, within a standard deviation of ~3 dB (Figure 4b). This curve indicates a positive but nonlinear relationship when MGS is finer than ~330 μm (medium sand), with a total increase of over 7 dB. There is likely a plateauing effect between MGS and backscatter return, when MGS is larger than ~330 μm.

Although the sorting variable was used by all of the 60 RFDT models, it was identified as an important sediment variable for backscatter response for a limited range of incidence angles only: 1–3°, 49–50°, 52–57°, and 59°. Among these, the predicted sorting-backscatter curves for incidence angles 1–3° are similar in shape with a standard deviation of 0.4 dB that describes a varying relationship between sorting and backscatter intensity (Figure 4c). Thus, for well-sorted sediment (sorting $<$~100 μm), backscatter intensity increases by about 1.7 dB toward slightly less well-sorted sediment. In the moderately sorted range (~100 to ~400 μm), sediments incur a uniformly strong backscatter intensity of ~$-$16 dB. In the poorly sorted range (~400 to ~650 μm), backscatter intensity decreases markedly to ~$-$30 dB for very poorly sorted sediment. For incidence angles greater than 49°, backscatter intensity follows a slightly different pattern with sediment sorting within a standard of ~1.5 dB, only with much weaker overall intensity (Figure 4d). Thus, the curve representing the mean of nine sorting-backscatter curves greater than 49° shows that when the sorting value is less

Table 2
Modeling Results Concerning the Sediment Variables

Measurement	%Mud	%Sand	%Gravel	MGS	Sorting	Kurtosis	Skewness
Times used by RFDT	60	34	55	52	60	54	5
Times identified as important	60	1	4	50	12	3	0
Min IS	100	0	0	0	35	0	0
Max IS	100	68	63	67	68	56	41
Mean IS	100	25.9	28.3	52.5	44.2	29.7	3.0

Note. MGS = mean grain size; IS = importance score.

than 250 μm, reduced sediment sorting only incurs a slight rise of backscatter intensity (~0.7 dB), further decreasing sediment sorting to ~550 μm sees an overall reduction of backscatter intensity by over 6 dB.

The kurtosis variable was identified as an important sediment variable for backscatter response between a narrow range of incidence angles between 55° and 57°. The predicted kurtosis-backscatter curves from these three models show similar shapes within a standard deviation of ~0.8 dB (Figure 4e). The mean kurtosis-backscatter curve indicates an initial steep decline of backscatter intensity of ~3.5 dB, when the kurtosis value increases from −1 to 5. This is followed by a gentle decline of over 2 dB in the kurtosis range of 6 and 26. Further increasing sediment kurtosis would not affect backscatter intensity. Between the kurtosis values of −1 and 26, the overall trend of the kurtosis-backscatter relationship is negative, with a total reduction of backscatter intensity by over 5 dB (Figure 4e).

The %gravel variable was identified as an important sediment variable for backscatter response between incidence angles of 57° and 60°. The predicted gravel-backscatter curves from these four models show more or less similar shapes within a narrow standard deviation of 1 dB (Figure 4f). The mean gravel-backscatter curve indicates an initial steep decline of backscatter intensity by over 6 dB, when sediment gravel content increases from 0% to 3%. Between sediment gravel content of 3% and 13%, there is a slight rise of ~0.3 dB, followed by a dip of ~1 dB to 16%. When sediment gravel content increases from16% to 100%, there is a very slow rise of ~2 dB.

The %sand variable was identified as an important sediment variable for backscatter response only at the incidence angle of 2°. The predicted sand-backscatter curve is displayed in Figure 4g. In general, when sand content is lower than 40%, increasing sediment sand content does not appear to affect backscatter intensity. Between sediment sand content of 40% and 60%, there is a steep rise of backscatter intensity by ~ 6 dB. Further increasing sand content in sediment would not further increase backscatter intensity.

6. Discussion

The backscatter strength at the water-sediment interface is controlled by five geoacoustic parameters; the sound velocity ratio (ν) and density ratio (ρ) parameters determine the acoustic impedance contrast (hardness); the loss parameter (δ) determines the sound attenuation (penetration) in sediments; the spectral strength (ω_2) and spectral exponent of bottom relief (γ) determine the interface roughness (Fonseca et al., 2002; Jackson et al., 1986). The volume backscatter, on the other hand, is controlled by the ratio of two parameters: the volume scattering cross-section parameter (σ_v) and the absorption parameter (a_b; Jackson et al., 1986). According to the geoacoustic model of Jackson et al. (1986) and some in situ measurements (e.g., Fonseca et al., 2002; Jackson & Briggs, 1992; Richardson & Briggs, 1996), the interface scattering increases with sediment grain size due to the increase of acoustic impedance contrast and roughness. The relationship between volume scattering and sediment grain size is a bit more complicated. According to equation (9) and Figure 19 in Hamilton (1980), there is a unimodal relationship between sediment grain size and absorption parameter (a_b). From very fine to medium-grained sediment, increasing grain size would increase the absorption parameter, but at the same time the scattering cross section would also increase due to the increase of sediment heterogeneity. Therefore, we can reasonably assume that the volume scattering due to σ_v and a_b would remain nearly constant in this range of sediment grain sizes. When sediment grain size increases from medium to very coarse, we would assume that the volume scattering σ_v and a_b would increase because of the decreasing absorption parameter in combination with increasing sediment heterogeneity (Hamilton,

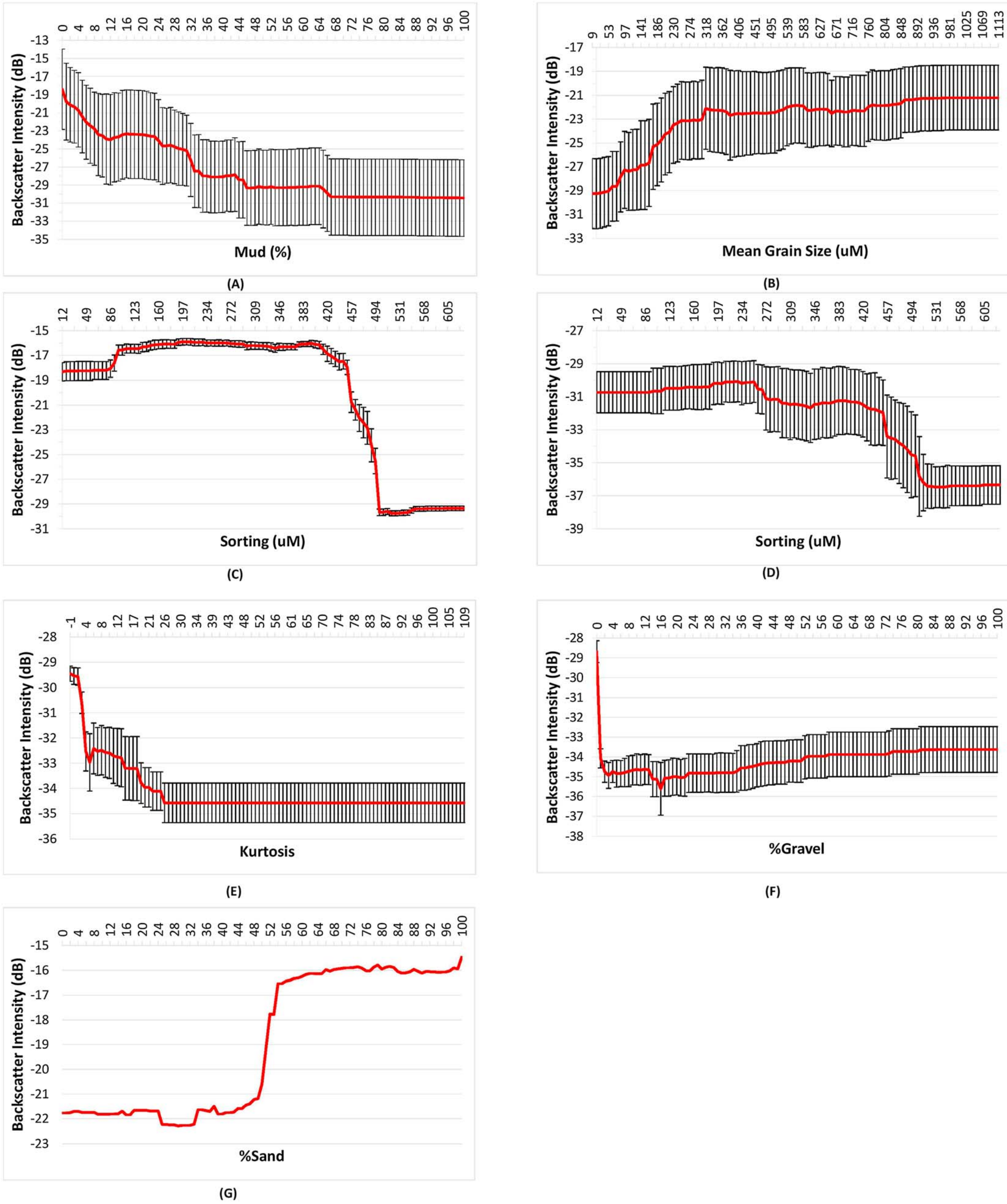

Figure 4. Predicted sediment-backscatter curves; (a) mean mud-backscatter curve for the incidence angles 1–60°; (b) mean grain size-backscatter curve for the incidence angles 2–51°; (c) mean sorting-backscatter curve for the incidence angles of 1–3°; (d) mean sorting-backscatter curve for the incidence angles of 49–50°, 52–57°, and 59°; the bars indicate the standard deviations; (e) mean kurtosis-backscatter curve for the incidence angles 55–57°; (f) mean gravel-backscatter curve for the incidence angles 57–60°; (g) sand-backscatter curve for the incidence angle of 2°; the bars indicate the standard deviations.

1980). However, the volume scattering actually received by the sonar is also strongly affected by the acoustic penetration (δ) into the sediment which in turn is controlled by sediment hardness, acoustic frequency, and sediment acoustic absorption (Jackson et al., 1986). In general, the volume scattering due to δ decreases with increased sediment grain size because of greater acoustic reflectivity (i.e., hardness). However, with the use of high-frequency energy (300 kHz) in this study, the acoustic penetration in coarse sediment is likely to be very limited (Richardson & Briggs, 1996; Simons & Snellen, 2008). As a result, from very fine to medium-grained sediment the total volume scattering due to σ_v, a_b, and δ is likely to decrease with the increasing MGS. When sediment grain size increases from medium to very coarse, the total volume scattering is either very small due to very limited acoustic penetration or remains nearly constant because the increasing volume scattering due to σ_v and a_b cancels out the decreasing acoustic penetration. The above explanation supports our finding of the initial clearly positive relationship and the subsequent plateauing effect or slightly positive relationship between sediment MGS and backscatter return, which is the combination of interface scattering and volume scattering (Figures 4b and 2d). This positive MGS-backscatter relationship is also supported by a number of previous studies (e.g., Collier & Brown, 2005; Davis et al., 1996; Ferrini & Flood, 2006; Goff et al., 2000; Huang, Siwabessy, et al., 2014; Ryan & Flood, 1996).

Similarly, the interface scattering decreases with the increase of sediment mud content due to the decrease of acoustic impedance contrast and roughness (Jackson et al., 1986). In sediment, increasing mud content would likely increase volume scattering due to δ because of greater acoustic penetration. This increase, however, would be limited, especially for coarse sediment with small mud content due to the use of high-frequency energy (300 kHz). In fine sediment, the increasing mud content would decrease both the volume scattering cross-section due to the decrease of sediment heterogeneity and the absorption (Hamilton, 1980), which likely results in nearly constant volume scattering due to σ_v and a_b. Therefore, in fine sediment, the increasing mud content would likely increase total volume scattering. In coarse sediment, volume scattering due to σ_v and a_b is likely to decrease with increasing mud content because of increasing absorption and decreasing cross-section scattering (Hamilton, 1980). This is likely to result in nearly constant or slightly decreasing total volume scattering with the increased mud content. Consequently, combining the contributions from the interface scattering and volume scattering would result in negative and flat (or slightly negative) relationships between sediment mud content and backscatter return in coarse and fine sediments, respectively. The finding of this study (Figures 4a and 2c) supports this explanation. Indeed, some of previous studies (e.g., De Falco et al., 2010; Goff et al., 2004; Huang, Siwabessy, et al., 2014; Sutherland et al., 2007) also support the negative Mud-Backscatter relationship.

Sediment sorting was the third most important variable resulted from the predictive modeling (Table 2). The sorting-backscatter relationships identified at near nadir and outer beams (Figures 4c and 4d) requires some interpretation. Both the univariate analysis at incidence angle of 25° and the predictive models at incidence angles 1–3° indicate that the sorting-backscatter relationship is likely to be unimodal (Figures 4c and 2e). Sorting (standard deviation) is a measure of sediment grain size heterogeneity. Decreased sediment sorting can be the result of greater proportions of either coarser grains or finer grains. In the case of increasing coarser grains, we would expect an increase in backscatter return, while in the case of increasing finer grains, we would expect a decrease in backscatter return. Neither case, however, explains the unimodal distribution observed, which is driven by samples with a backscatter intensity in the range -30 to -50 dB (Figure 5a). The majority of the samples in this very low backscatter range are from the Oceanic Shoals study area where mud content is highest among all the study areas. Removing the Oceanic Shoals samples results in a nearly flat or slightly positive sorting-backscatter relationship, with a poor correlation (Figure 5b), while the Oceanic Shoals samples alone have a much stronger positive sorting-backscatter relationship (Figure 5c). This we attribute to the higher mud content (47 ± 21%) than those in the other three study areas (9 ± 12%). At small incidence angles (1–3°; near nadir), backscatter strength is dominated by the impedance contrast (or hardness), but this decreases very quickly with soft sediment (Ferrini & Flood, 2006; Jackson et al., 1986). This of course explains the much lower backscatter intensity of these muddy samples (Figure 5c). Therefore, we can reasonably state that a unimodal sorting-backscatter relationship (with flat top in the moderately sorted range) is plausible provided that a sufficient number of samples with diverse grain size properties are used to derive the relationship, a key advantage of this study. Using only samples from one local area may result in a misleading sorting-backscatter relationship. At the outer beams, beyond the critical angle, interface scattering due to roughness is becoming the sole contributor to backscatter strength (Jackson et al., 1986; Jackson & Briggs, 1992). Decreased sediment sorting, if it is the result of increased mud content, would reduce backscatter intensity because of the decreasing interface roughness. For the Oceanic Shoals muddy samples that have much lower backscatter intensity, this could again lead to the negative Sorting-Backscatter relationship in Figure 4d after 250 μm.

Statistically, kurtosis measures the tailedness of the probability distribution. Higher kurtosis indicates heavier tails. For our sediment data sets, samples with larger kurtosis are more likely tailed towards higher mud content because of the positive relationship between kurtosis and mud content ($r = 0.42$). This thus could explain the negative kurtosis-backscatter relationships identified in Figures 2f and 4e, which was predicted at outer beams.

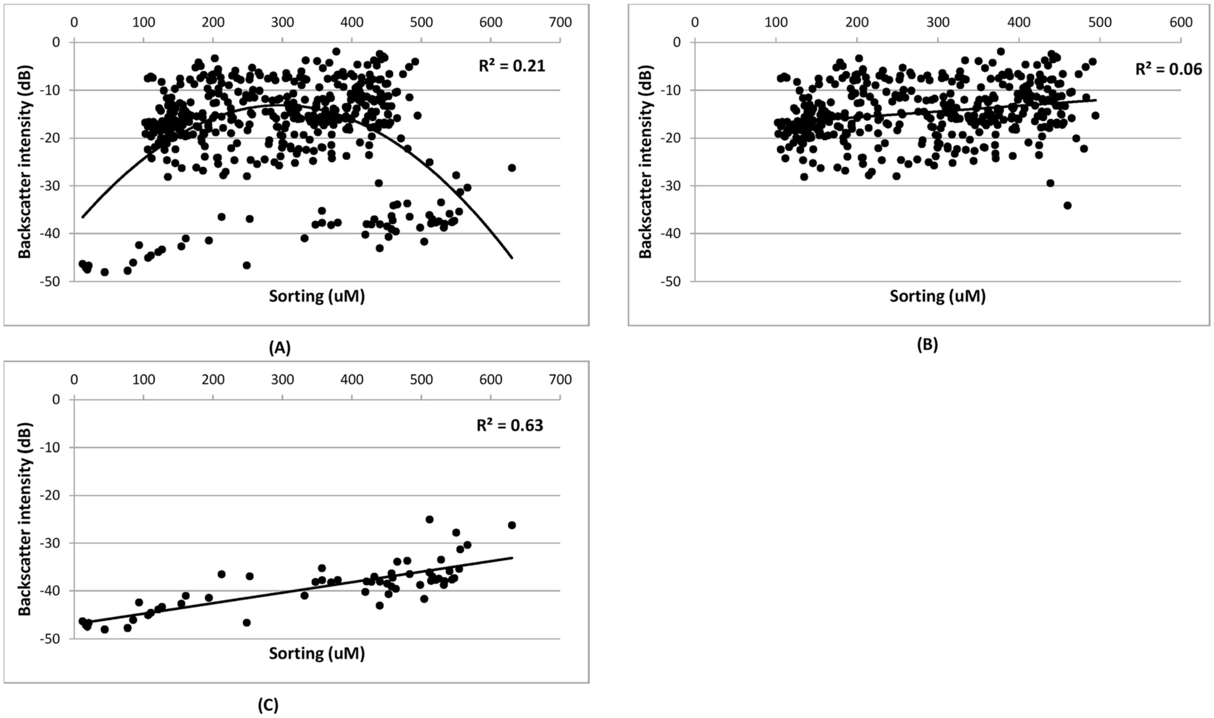

Figure 5. Scatter plots between sorting and backscatter intensity at the incidence angle of 1°; (a) samples from all four study areas; (b) samples from three study areas except Oceanic Shoals; (c) samples from the study area of Oceanic Shoals.

In this study, among all sediment properties, gravel content has the lowest correlation with backscatter intensity (Figure 2a). The gravel content was identified as an important contributor to backscatter intensity only at the farthest end of the outer beams (57–60°). The general trend of a positive gravel-backscatter relationship (Figures 2 and 4f) is reasonable because of the increased interface scattering with higher gravel content. However, the steep and uncharacteristic dip of backscatter intensity at lower gravel content ($<$3%), predicted by the model, could not be reasonably explained. The overall result in this study indicates that gravel content is not a good predictor of backscatter intensity. A much larger data set and further studies, however, are required to validate this implication.

The sand-backscatter relationship identified at the incidence angle of 2° seems to indicate a boundary condition of around 50% sand content, above which the backscatter return is strong and below which the backscatter return is around 6 dB weaker (Figure 4g). Examining the data reveals that, in general, the sediment samples with less than 50% sand content have much higher mud content (37 ± 33%) than those samples with more than 50% sand content (8 ± 10%). This could explain the sand-backscatter relationship identified at this nadir angle (Figure 4g).

The above findings clearly indicate that mud content plays a key role in sediment-acoustic relationship. This is consistent with the fact that the %mud variable was the most important sediment variable controlling the backscatter return (Table 2). Importantly, in this data set the %mud variable alone explains around 40% of predictive variance for the incidence angles smaller than 41° (Figure 3). With the addition of MGS the predictive variance at this incidence angle range increases to 60% (Figure 3). Adding the remaining sediment variables only achieves minor improvements in model performance (Figure 3). On the other hand, at large incidence angles, especially beyond the critical angle, the model performance degraded quickly and the predicted sediment-backscatter relationships become less reliable. It is therefore reasonable to assume that the sediment-acoustic relationship is mostly due to the combined influence of sediment mud content and MGS.

To examine how the interaction between the sediment mud content and MGS affects the acoustic backscatter response, a two-variable (%mud + MGS) RFDT model was generated for the incidence angle of 25°. The model explained 61.6% of the variance, with the variable ISs of 100 and 72 for the %mud and the MGS variable, respectively. An artificial 10×10 data matrix (%mud: 5, 15, 25, …, 95; MGS: 50, 150, 250, …, 950 μm) was

10.1029/2017JC013638

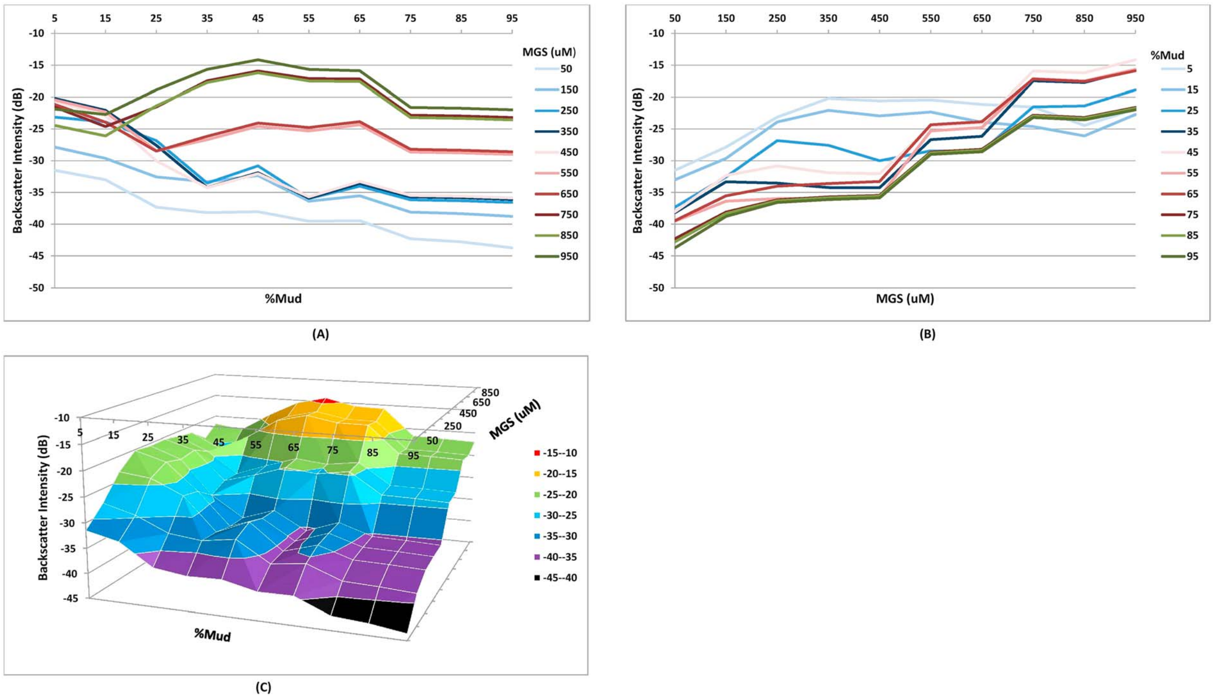

Figure 6. The influence of the interaction of sediment mud content and mean grain size (MGS) on the backscatter intensity; (a) the influence of sediment MGS on the mud-backscatter relationships; (b) the influence of sediment mud content on the MGS-backscatter relationships; (c) 3-D surface plot on the mud-backscatter and MGS-backscatter relationships.

fed to the model to predict the backscatter intensity values. Figure 6a indicates that sediment MGS influences the mud-backscatter relationship, for example, when sediment MGS is larger than 450 μM, the %mud-backscatter relationship is no longer negative but unimodal. On the other hand, sediment mud content also influences the MGS-backscatter relationship, for example, when mud content is larger than 25%, a clearly positive MGS-backscatter relationship was found within the entire range of sediment MGSs instead of a plateau effect found for smaller mud content (Figure 6b). The 3-D surface plot (Figure 6c) clearly shows that the strongest backscatter return occurs for muddy coarse sand (35–65% mud and MGS $> = 750$ μm) and the weakest backscatter return occurs for silty mud ($> = 75$% mud and MGS <50 μm).

Apart from %mud and MGS, which were identified as important variables across most incidence angles, other sediment variables were identified as important either at near nadir (%sand and sorting) or at outer beams (%gravel, sorting, and kurtosis; Figure 4). The acoustic physics underlying the backscatter intensity at near nadir and outer beams is well known (e.g., Hamilton, 1980; Jackson et al., 1986). However, due to the relatively narrow angular ranges within which these sediment variables were identified as important, we require caution in the interpretation of the sorting-backscatter, kurtosis-backscatter, gravel-backscatter, and sand-backscatter relationships offered above. In particular, the backscatter strength decreases quickly in the outer beam range, which reduces the signal-to-noise ratio. Indeed, the gradual decrease of OOB R^2 values beyond 41° (Figure 3) was likely due to the reduction of the signal-to-noise ratio. This relatively low signal-to-noise ratio could raise some uncertainty over the sediment-backscatter relationships predicted at the outer beam range (Figures 4d–4f).

7. Conclusion

This study demonstrates the effectiveness of a multivariate statistical approach for the investigation of the sediment-acoustic relationship. Using a large sample set of colocated sediment and multibeam backscatter data collected from diverse sedimentary environments has allowed us to examine the sediment-acoustic relationship across a wide range of physical properties. The key findings of this study include the following:

1. Sediment mud content is the most important sediment variable and has a significant negative relationship with backscatter intensity.

2. Sediment MGS is the second ranked sediment variable and has a positive relationship with backscatter intensity.
3. Sediment mud content also plays a key role in sorting-backscatter and %sand-backscatter relationships.
4. For incidence angles between 1° and 41°, the sediment variables explain around 70% of variance in the backscatter intensity.
5. The combined influence of sediment mud content and MGS can largely explain the sediment-acoustic relationship.
6. The strongest backscatter return occurs with medium sediment mud content and large MGSs (or muddy coarse sand).
7. The sediment-acoustic relationship beyond the critical angle could not been reliably resolved.

It should be noted that the seven sediment grain size properties used in this study are only proxies of the sediment geoacoustic parameters including sound velocity, density, absorption, roughness, and volume heterogeneity. It is likely that this use of proxies instead of direct drivers has accounted for a proportion of the unexplained variance in the modeling accuracy. The potential violation of the homogeneity assumption within the 30-m buffers of some sediment sample locations may also contribute to some of the unexplained variance. The relatively high modeling accuracy (~70% of variance explained), however, indicates that sediment grain size properties are effective proxies of geoacoustic parameters. Importantly, the sediment grain size properties can be measured much more easily than other sediment properties. In fact, the sediment grain size properties have been routinely collected during marine surveys. This creates opportunities for wider application of the statistical approach used in this study for the future more comprehensive investigation of sediment-acoustic relationship.

Acknowledgments
This work was supported by the Open Research Fund of State Key Laboratory of Estuarine and Coastal Research, East China Normal University (grant SKLEC-KF201504). Kim Pichard and Brendan Brooke of Geoscience Australia provided valuable comments that improved the manuscript. We would like to thank two anonymous reviewers for their constructive comments. This paper is published with permission of the Chief Executive Officer, Geoscience Australia. Data used in this work are available in the supporting information.

References

Anderson, J. T., Holliday, D. V., Kloser, R., Reid, D. G., & Simard, Y. (2008). Acoustic seabed classification: Current practice and future directions. *ICES Journal of Marine Science*, *65*(6), 1004–1011. https://doi.org/10.1093/icesjms/fsn061

Anderson, T., Brooke, LB., Radke, L., McArthur, M., & Hughes, M. (2009). Mapping and characterising soft-sediment habitats, and evaluating physical variables as surrogates of biodiversity in Jervis Bay, NSW. Geoscience Australia, Record 2009/10. Geoscience Australia, Canberra, 43 pp.

APL-UW (1994). *High-frequency ocean environmental acoustic models handbook (APL-UW TR 9407)*. Seattle, WA: Applied Physics The Laboratory, University of Washington.

Blott, S. J., & Pye, K. (2001). GRADISTAT: A grain size distribution and statistics package for the analysis of unconsolidated sediments. *Earth Surface Processes and Landforms*, *26*(11), 1237–1248. https://doi.org/10.1002/esp.261

Breiman, L. (2001). Random forests. *Machine Learning*, *45*(1), 5–32. https://doi.org/10.1023/A:1010933404324

Breiman, L., Friedman, J. H., Olshen, R. A., & Stone, C. J. (1984). *Classification and regression trees* (p. 358). Monterey: Brooks/Cole Publishing.

Brooke, B., Nichol, S., Hughes, M., McArthur, M., Anderson, T., Przeslawski, R., et al. (2009). Carnarvon shelf survey post-survey report. Geoscience Australia, Record 2009/02, 90 pp.

Buchanan, C., Spinoccia, M., Picard, K., Wilson, O., Sexton, M. J, Hodgkin, S., et al. (2013). Standard operation procedure for a multibeam survey: Acquisition & processing. Record 2013/33. Geoscience Australia: Canberra.

Chakraborty, B., Schenke, H. W., Kodagali, V., & Hagen, R. (2000). Seabottom characterization using multibeam Echosounder angular backscatter: An application of the composite roughness theory. *IEEE Transactions on Geoscience and Remote Sensing*, *38*(5), 2419–2422. https://doi.org/10.1109/36.868896

Collier, J. S., & Brown, C. J. (2005). Correlation of sidescan backscatter with grain size distribution of surficial seabed sediments. *Marine Geology*, *214*(4), 431–449. https://doi.org/10.1016/j.margeo.2004.11.011

Davis, K. S., Slowey, N. C., Stender, I. H., Fiedler, H., Bryant, W. R., & Fechner, G. (1996). Acoustic backscatter and sediment textural properties of inner shelf sands, northeastern Gulf of Mexico. *Geo-Marine Letters*, *16*(3), 273–278. https://doi.org/10.1007/BF01204520

De, C., & Chakraborty, B. (2011). Model-based acoustic remote sensing of seafloor characteristics. *IEEE Transactions on Geoscience and Remote Sensing*, *49*(10), 3868–3877. https://doi.org/10.1109/TGRS.2011.2139218

De Falco, G., Tonielli, R., Di Martino, G., Innangi, S., Simeone, S., & Parnum, I. M. (2010). Relationships between multibeam backscatter, sediment grain size and *Posidonia oceanica* seagrass distribution. *Continental Shelf Research*, *30*(18), 1941–1950. https://doi.org/10.1016/j.csr.2010.09.006

de Moustier, C., & Alexandrou, D. (1991). Angular dependence of 12-kHz seafloor acoustic backscatter. *The Journal of the Acoustical Society of America*, *90*(1), 522–531. https://doi.org/10.1121/1.401278

de Moustier, C., & Matsumoto, H. (1993). Seafloor acoustic remote sensing with multibeam echo-sounders and bathymetric sidescan sonar systems. *Marine Geophysical Researches*, *15*(1), 27–42. https://doi.org/10.1007/BF01204150

Ferrini, V. L., & Flood, R. D. (2006). The effects of fine-scale surface roughness and grain size on 300 kHz multibeam backscatter intensity in sandy marine sedimentary environments. *Marine Geology*, *228*, 153–172. https://doi.org/10.1016/j.margeo.2005.11.010

Fonseca, L., Mayer, L., Orange, D., & Driscoll, N. (2002). The high-frequency backscattering angular response of gassy sediments: Model/data comparison from the Eel River Margin, California. *The Journal of the Acoustical Society of America*, *111*(6), 2621–2631. https://doi.org/10.1121/1.1471911

Fonseca, L., & Mayer, L. A. (2007). Remote estimation of surficial seafloor properties through the application Angular Range Analysis to multibeam sonar data. *Marine Geophysical Researches*, *28*(2), 119–126. https://doi.org/10.1007/s11001-007-9019-4

Francke, T., Lopez-Tarazon, J. A., & Schroder, B. (2008). Estimation of suspended sediment concentration and yield using linear models, random forests and quantile regression forests. *Hydrological Processes*, *22*(25), 4892–4904. https://doi.org/10.1002/hyp.7110

Gavrilov, A. N., Duncan, A. J., McCauley, R. D., Parnum, I. M., Penrose, J. D., Siwabessy, P. J. W., et al. (2005). Characterization of the seafloor in Australia's coastal zone using acoustic techniques. Proceedings of the International Conference in Underwater Acoustic Measurements: Technologies & Results, Crete, Greece.

Gavrilov, A.N., Siwabessy, P. J. W., & Parnum, I. M. (2005). Multibeam echo sounder backscatter analysis: Theory review, methods and application to Sydney Harbour swath data. CRC Milestone Report CA3.03. CMST Report 2005–03 for the Cooperative Research Centre for Coastal Zone, Estuary and Waterway Management, Centre for Marine Science and Technology, Curtin University of Technology.

Goff, J. A., Kraft, B. J., Mayer, L., Schock, S. G., Sommerfield, C. K., Olson, H. C., et al. (2004). Seabed characterization on the New Jersey middle and outer shelf: Correlatability and spatial variability of seafloor sediment properties. *Marine Geology*, *209*(1-4), 147–172. https://doi.org/10.1016/j.margeo.2004.05.030

Goff, J. A., Olson, H. C., & Duncan, C. S. (2000). Correlation of side-scan backscatter intensity with grain-size distribution of shelf sediments, New Jersey margin. *Geo-Marine Letters*, *20*(1), 43–49. https://doi.org/10.1007/s003670000032

Gogina, M., Glockzin, M., & Zettler, M. L. (2010). Distribution of benthic macrofaunal communities in the western Baltic Sea with regard to near-bottom environmental parameters. 2. Modelling and prediction. *Journal of Marine Systems*, *80*(1-2), 57–70. https://doi.org/10.1016/j.jmarsys.2009.10.001

Hamilton, E. L. (1980). Geoacoustic modeling of the sea floor. *The Journal of the Acoustical Society of America*, *68*(5), 1313–1340. https://doi.org/10.1121/1.385100

Hamilton, L. J., & Parnum, I. M. (2011). Acoustic seabed segmentation from direct statistical clustering of entire multibeam sonar backscatter curves. *Continental Shelf Research*, *31*(2), 138–148. https://doi.org/10.1016/j.csr.2010.12.002

Hammerstad, E. (2000). EM Technical Note: Backscattering and Seabed Image Reflectivity. Kongsberg Technical Documentation.

Haris, K., Chakraborty, B., Chanchal, D., Prabhudesai, R. G., & Willam, F. (2011). Model-based seafloor characterization employing multi-beam angular backscatter data—A comparative study with dual-frequency single beam. *The Journal of the Acoustical Society of America*, *130*(6), 3623–3632. https://doi.org/10.1121/1.3658454

Haris, K., Chakraborty, B., Ingole, B., Menezes, A., & Srivastava, R. (2012). Seabed habitat mapping employing single and multi-beam backscatter data: A case study from the western continental shelf of India. *Continental Shelf Research*, *48*, 40–49. https://doi.org/10.1016/j.csr.2012.08.010

Heap, A.D., Przeslawski, R., Radke, L., Trafford, J., Battershill, C., & Shipboard Party. (2010). Seabed environment of the eastern Joseph Bonaparte Gulf, Northern Australia. SOL 4934—Post-survey report. Geoscience Australia, Record 2010/09, 78pp.

Holloway, P. E., Symonds, G., & Nunes Vaz, R. (1992). Observations of circulation and exchange processes in Jervis Bay, New South Wales. *Australian Journal of Marine and Freshwater Research*, *43*(6), 1487–1515. https://doi.org/10.1071/MF9921487

Huang, Z., McArthur, M., Przeslawski, R., Siwabessy, P. J. W., Nichol, S., Anderson, T., & Brooke, B. (2014). Predicting mapping of soft bottom benthic biodiversity using a surrogacy approach. *Marine and Freshwater Research*, *65*(5), 409–424. https://doi.org/10.1071/MF13104

Huang, Z., Nichol, S. L., Siwabessy, J., Daniell, J., & Brooke, B. P. (2012). Predictive modelling of seabed sediment parameters using multibeam acoustic data: A case study on the Carnarvon Shelf, Western Australia. *International Journal of Geographical Information Science*, *26*(2), 283–307. https://doi.org/10.1080/13658816.2011.590139

Huang, Z., Siwabessy, J., Nichol, S. L., Anderson, T., & Brooke, B. (2013). Predictive mapping of seabed cover types using angular response curves of multibeam backscatter data: Testing different feature analysis approaches. *Continental Shelf Research*, *61-62*, 12–22. https://doi.org/10.1016/j.csr.2013.04.024

Huang, Z., Siwabessy, J., Nichol, S. L., & Brooke, B. P. (2014). Predictive mapping of seabed substrata using high-resolution multibeam sonar data: A case study from a shelf with complex geomorphology. *Marine Geology*, *357*, 37–52. https://doi.org/10.1016/j.margeo.2014.07.012

Hughes Clarke, J. E. (1994). Toward remote seafloor classification using the angular response of acoustic backscattering: A case study from multiple overlapping GLORIA data. *IEEE Journal of Oceanic Engineering*, *19*(1), 112–127. https://doi.org/10.1109/48.289456

ICES (2007). Acoustic Seabed Classification of Marine Physical and Biological Landscapes Cooperative Research Report No. 286. International Council for the Exploration of the Sea (ICES) (183 pp.).

Jackson, D. R., & Briggs, K. B. (1992). High-frequency bottom backscattering: Roughness versus sediment volume scattering. *The Journal of the Acoustical Society of America*, *92*(2), 962–977. https://doi.org/10.1121/1.403966

Jackson, D. R., Winebrenner, D. P., & Ishimaru, A. (1986). Application of the composite roughness model to high-frequency bottom backscattering. *The Journal of the Acoustical Society of America*, *79*(5), 1410–1422. https://doi.org/10.1121/1.393669

Kloser, R. J., Bax, N., Ryan, J. T., Williams, A., & Barker, B. A. (2001). Remote sensing of seabed types in the Australian South East Fishery; development and application of normal incident acoustic techniques and associated 'ground truthing. *Marine and Freshwater Research*, *52*(4), 475–489. https://doi.org/10.1071/MF99181

Lamarche, G., & Lurton, X. (2017). Recommendations for improved and coherent acquisition and processing of backscatter data from seafloor-mapping sonars. *Marine Geophysical Research*, *39*(1-2), 5–22. https://doi.org/10.1007/s11001-017-9315-6

Lamarche, G., Lurton, X., Verdier, A. L., & Augustin, J. M. (2011). Quantitative characterisation of seafloor substrate and bedforms using advanced processing of multibeam backscatter-application to Cook Strait, New Zealand. *Continental Shelf Research*, *31*(2), s93–s109. https://doi.org/10.1016/j.csr.2010.06.001

Lees, B. G. (1992). Recent terrigenous sedimentation in Joseph Bonaparte Gulf, northwestern Australia. *Marine Geology*, *103*(1-3), 199–213. https://doi.org/10.1016/0025-3227(92)90016-B

Lewis, D. W., & McConchie, D. (1994). *Analytical Sedimentology*. New York: Chapman & Hall.

Lucieer, V. L. (2008). Object-oriented classification of sidescan sonar data for mapping benthic marine habitats. *International Journal of Remote Sensing*, *29*(3), 905–921. https://doi.org/10.1080/01431160701311309

Lucieer, V. L., & Lamarche, G. (2011). Unsupervised fuzzy classification and object-based image analysis of multibeam data to map deepwater substrates, CookStrait, NewZealand. *Continental Shelf Research*, *31*(11), 1236–1247. https://doi.org/10.1016/j.csr.2011.04.016

Lurton, X., & Lamarche, G. (2015). Backscatter measurements by seafloor-mapping sonars. Guidelines and Recommendations. In

McGonigle, C., Brown, C., Quinn, R., & Grabowski, J. (2009). Evaluation of image-based multibeam sonar backscatter classification for benthic habitat discrimination and mapping at Stanton Banks, UK. *Estuarine, Coastal and Shelf Science*, *81*(3), 423–437. https://doi.org/10.1016/j.ecss.2008.11.017

Nichol, S. L., & Brooke, B. (2011). Shelf habitat distribution as a legacy of Late Quaternary marine transgressions: A case study from a tropical carbonate province. *Continental Shelf Research*, *31*(17), 1845–1857. https://doi.org/10.1016/j.csr.2011.08.009

Nichol, S. L., Howard, F. J. F., Kool, J., Stowar, M., Bouchet, P., Radke, L., et al. (2013). Oceanic Shoals Commonwealth Marine Reserve (Timor Sea) biodiversity survey: GA0339/SOL5650—Post survey report. Record 2013/38. Geoscience Australia: Canberra.

Parnum, I. M., & Gavrilov, A. N. (2011a). High-frequency multibeam echo-sounder measurements of seafloor backscatter in shallow water: Part 1—Data acquisition and processing. *International Journal of the Society for Underwater Technology*, *30*(1), 3–12. https://doi.org/10.3723/ut.30.003

Parnum, I. M., & Gavrilov, A. N. (2011b). High-frequency multibeam echo-sounder measurements of seafloor backscatter in shallow water: Part 2—Mosaic production, analysis and classification. *International Journal of the Society for Underwater Technology*, *30*(1), 13–26. https://doi.org/10.3723/ut.30.013

Pratson, L. E., & Edwards, M. H. (1996). Introduction to advances in seafloor mapping using sidescan sonar and multibeam bathymetry data. *Marine Geophysical Researches*, *18*(6), 601–605. https://doi.org/10.1007/BF00313876

Preston, J. (2009). Automated acoustic seabed classification of multibeam images of Stanton Banks. *Applied Acoustics*, *70*(10), 1277–1287. https://doi.org/10.1016/j.apacoust.2008.07.011

Przeslawski, R., Daniell, J., Anderson, T., Barrie, J.V., Heap, A., Hughes, M., et al. (2011). Seabed habitats and hazards of the Joseph Bonaparte Gulf and Timor Sea, Northern Australia. Geoscience Australia, Record 2011/40, 69pp.

Richardson, M. D., & Briggs, K. B. (1996). In situ and laboratory geoacoustic measurements in soft mud and hard-packed sand sediments: Implications for high-frequency acoustic propagation and scattering. *Geo-Marine Letters*, *16*(3), 196–203. https://doi.org/10.1007/BF01204509

Ryan, W. B. E., & Flood, R. D. (1996). Side-looking sonar backscatter response at dual frequencies. *Marine Geophysical Researches*, *18*(6), 689–705. https://doi.org/10.1007/BF00313881

Rzhanov, Y., Fonseca, L., & Mayer, L. (2012). Construction of seafloor thematic maps from multibeam acoustic backscatter angular response data. *Computers & Geosciences*, *41*, 181–187. https://doi.org/10.1016/j.cageo.2011.09.001

Sherrod, P. H. (2008). DTREG [online]. Retrieved from http://www.dtreg.com (accessed October 12, 2011).

Simons, D.G., & Snellen, M. (2008). A comparison between modeled and measured high frequency bottom backscattering. In, *Acoustics 08*. Paris, France

Siwabessy, P. J. W., Tran, M., Picard, K., Brooke, B. P., Huang, Z., Smit, N., et al. (2017). Modelling the distribution of hard seabed using calibrated multibeam acoustic backscatter data in a tropical, macrotidal embayment: Darwin Harbour, Australia. *Marine Geophysical Research*, *39*, 249–269. https://doi.org/10.1007/s11001-017-9314-7

Sutherland, T. F., Galloway, J., Loschiavo, R., Levings, C. D., & Hare, R. (2007). Calibration techniques and sampling resolution requirements for groundtruthing multibeam acoustic backscatter (EM3000) and QTC VIEW classification technology. *Estuarine, Coastal and Shelf Science*, *75*(4), 447–458. https://doi.org/10.1016/j.ecss.2007.05.045

Taylor, G. (1972). Sedimentation in Jervis Bay. *Proceedings of the Linnean Society of New South Wales*, *96*, 297–306.